Raman phonon spectrum of the Dzyaloshinskii-Moriya helimagnet $Ba_2CuGe_2O_7$

F. Capitani,[1] S. Koval,[2] R. Fittipaldi,[3] S. Caramazza,[1] E. Paris,[4] W. S. Mohamed,[1] J. Lorenzana,[5] A. Nucara,[6] L. Rocco,[3] A. Vecchione,[3] P. Postorino,[1] and P. Calvani[6]

[1]*Dipartimento di Fisica, Università di Roma "La Sapienza," Piazzale A. Moro 2, 00185 Rome, Italy*
[2]*Instituto de Física Rosario, Universidad Nacional de Rosario, 27 de Febrero 210 Bis, 2000 Rosario, Argentina*
[3]*CNR-SPIN and Dipartimento di Fisica "E. R. Caianiello," Via Giovanni Paolo II 132, 84084 Fisciano, Salerno, Italy*
[4]*Center for Life Nano Science at Sapienza, Istituto Italiano di Tecnologia, Viale Regina Elena 291, 00186, Rome, Italy*
[5]*CNR-ISC and Dipartimento di Fisica, Università di Roma "La Sapienza," Piazzale A. Moro 2, 00185 Rome, Italy*
[6]*CNR-SPIN and Dipartimento di Fisica, Università di Roma "La Sapienza," Piazzale A. Moro 2, 00185 Rome, Italy*

(Received 2 April 2015; revised manuscript received 2 June 2015; published 22 June 2015)

The Raman spectrum of $Ba_2CuGe_2O_7$, a tetragonal insulator which develops Dzyaloshinskii-Moriya helical magnetism below $T_N = 3.2$ K, has been detected at temperatures varying from 300 to 80 K in a single crystal, with the radiation polarized either in the *ab* plane or along the *c* axis of its tetragonal cell. Twenty-nine phonon lines out of the 35 allowed by the Raman selection rules for the present geometry were observed, and their vibrational frequencies were found in overall good agreement with those provided by shell-model calculations. Together with the previous report on the infrared-active phonons [A. Nucara *et al.*, Phys. Rev. B **90**, 014304 (2014)], the present study provides an exhaustive description, both experimental and theoretical, of the lattice dynamics in $Ba_2CuGe_2O_7$.

DOI: 10.1103/PhysRevB.91.214308 PACS number(s): 78.30.Hv, 63.20.−e

I. INTRODUCTION

$Ba_2CuGe_2O_7$ (BCGO) is an insulating oxide that has recently been the object of several studies following the discovery that it develops helical magnetism at liquid-helium temperatures [1–3] via the Dzyaloshinskii-Moriya (DM) mechanism [4,5]. This behavior is unique even in the $Ba_2XGe_2O_7$ family, as the members with X = Mn or Co are magnetoelectric antiferromagnets (AF) at low temperatures. Below $T_N = 3.2$ K, BCGO displays a quasi-AF cycloidal, incommensurate magnetism, and despite the absence of a center of inversion symmetry in the crystal structure, it does not display spontaneous ferroelectricity [6]. Nevertheless, BCGO is usually considered a multiferroic material because it develops macroscopic electric polarization in an external magnetic field [7]. Figure 1 shows [2] its noncentrosymmetric tetragonal unit cell (space group [8] $P\bar{4}2_1m$), which corresponds to two formula units. The lattice parameters are $a = b = 0.8466$ nm and $c = 0.5445$ nm at room temperature. The layers made of corner-sharing GeO_4 and CuO_4 tetrahedra are separated by Ba^{2+} planes. A square lattice of Cu^{2+} ions thus results, where below T_N the Cu spins interact with each other through the DM mechanism producing the helical magnetic structure. The infrared spectra did not reveal any structural transition between 7 and 300 K. A strong enhancement of the infrared intensity at low temperature was detected instead, which suggests a redistribution of the electron charge in the unit cell with a possible increase of the dielectric constant [10]. It is worth noting that strong effects on the infrared phonon lines were observed at low temperature on the (under)doped Cu-O planes of high-T_c superconductors [11]. Therein, like in the present case, the charges move in a two-dimensional, strongly polar environment.

This work is aimed at completing the description of the lattice dynamics in BCGO by presenting its Raman phonon spectrum from both experimental observations and shell-model calculations.

II. EXPERIMENT AND RESULTS

Single crystals of $Ba_2CuGe_2O_7$ were grown and characterized as described in Ref. [12]. The surface exposed to the radiation was $a - c$ or $b - c$, as the a and b axes are degenerate. In the following, we shall conventionally assume that it was $a - c$.The Raman spectra were measured with a Horiba LabRAM HR Evolution microspectrometer in backscattering geometry. Samples were excited by the 632.8-nm radiation of a He-Ne laser with 30 mW of linearly polarized output power. Polarization rotators, properly located along the internal optical path, allowed us to align the electric field $\vec{E}$ of the incident beam either along the crystalline axis a or along c. We did not place an analyzer on the path of the backscattered radiation as the grating itself, once tested on the 520 cm^{-1} phonon of a Si crystal, showed a filtering efficiency of about 80% in the direction orthogonal to the grooves. By also taking into account the rather large numerical aperture of the microscope, we assumed a (partially) mixed scattering configuration. Therefore the assignment of the Raman lines was based not only on the selection rules but also on the shell-model calculations and on a comparison with the infrared spectra of Ref. [10]. The elastically scattered light was removed by a state-of-the-art optical filtering device based on three BragGrate notch filters [13]. Raman spectra in the 10–1000 cm^{-1} range were thus collected by a Peltier-cooled charge-coupled device (CCD) detector with a spectral resolution better than 1 cm^{-1} thanks to a grating with 1800 grooves/mm with a 800-mm focal length. Measurements were performed with a long-working-distance 20× objective (numerical aperture of 0.35). The sample was mounted on the cold finger of a liquid-nitrogen-cooled horizontal cryostat by Oxford Instruments, and the measurements were carried out in the 80–300 K temperature range. The system was thermoregulated by platinum thermometers, one of which was located very close to the sample. We thus obtained thermal stability within ±2 K during data collection at each working temperature.

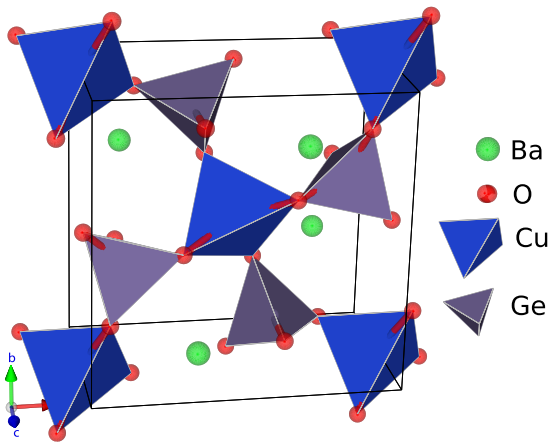

FIG. 1. (Color online) Lattice structure of $Ba_2CuGe_2O_7$ (reelaborated from Ref. [8] with the graphical tools reported in Ref. [9]). The oxygen tetrahedra contain a copper atom if blue and a germanium atom if gray.

The results of Raman scattering in $Ba_2CuGe_2O_7$ are shown in Fig. 2 for the radiation polarized along the a axis and in Fig. 3 for the electric field along the c axis. For the sake of clarity,

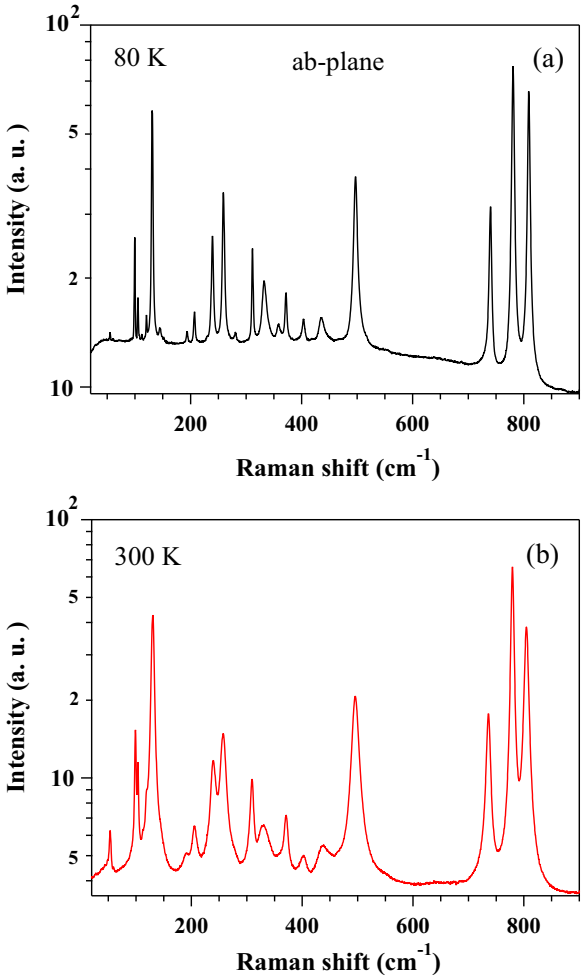

FIG. 2. (Color online) Raman spectrum of $Ba_2CuGe_2O_7$ at (a) 80 K and (b) 300 K, with the incident radiation polarized along the a axis. The spectra are not corrected for the temperature.

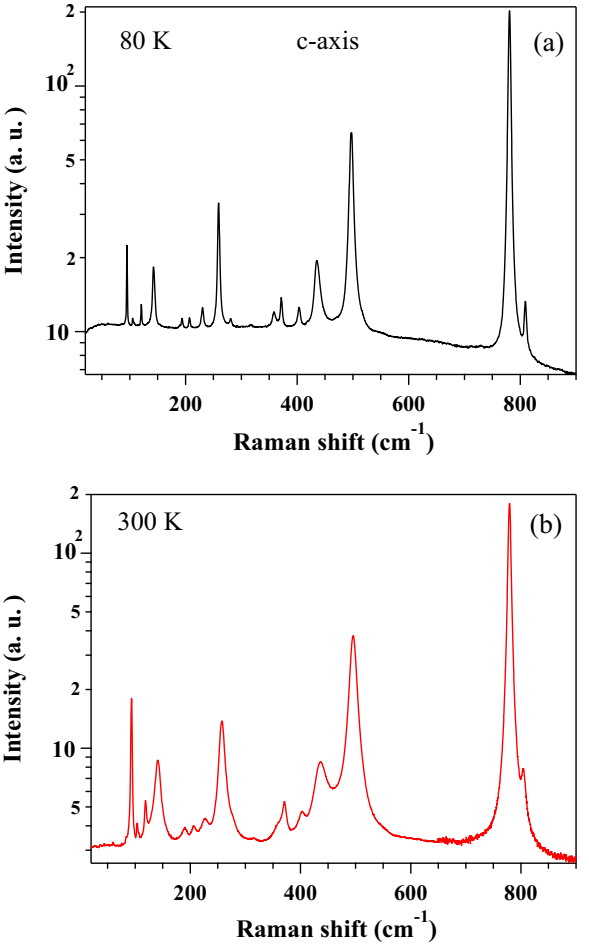

FIG. 3. (Color online) Raman spectrum of $Ba_2CuGe_2O_7$ at (a) 80 K and (b) 300 K, with the incoming radiation polarized along the c axis. Nine of these lines also appear in the spectra of Fig. 2. The spectra are not corrected for the temperature.

only spectra taken at 80 and 300 K are reported, as no major effects were found to affect the phonon lines at intermediate temperatures. In order to assign the observed spectral features we start from the factor-group analysis, which predicts for the $P\bar{4}2_1m$ unit cell of $Ba_2CuGe_2O_7$ the vibrational representation

$$R = 10A_1 + 6A_2 + 7B_1 + 11B_2 + 19E, \qquad (1)$$

where the E modes are doubly degenerate. After excluding the acoustic phonons (one B_2 and one E) and the 6 A_2 silent modes, one is left with 45 optical phonons, which, due to the lack of inversion symmetry, are, in principle, all Raman active: the 18 E and 10 A_1 vibrations of the ab plane and the 7 B_1 and 10 B_2 modes of the c axis. However, as the wave vector of the incoming radiation is aligned along the crystalline axis b, the selection rules for $P\bar{4}2_1m$ exclude the Raman lines of B_2 symmetry with $\vec{E}$ along both a and c [14]. The B_2 phonons are also infrared active (as the E ones), and most of them were reported in Ref. [10]. In Fig. 2 we detect, at 80 K, 24 lines with $\vec{E}$ along a (two of which are extracted from a couple of asymmetric lines by fitting to the data a sum of Lorentzians), while 17 lines are observed with $\vec{E}$ along the c axis in Fig. 3. Among the latter ones, however, only five are not replicas of those of the ab plane. Indeed, in the present geometry the

TABLE I. All the Raman phonon frequencies Ω_j^R, linewidths Γ_j^R, and relative intensities S_j^R observed in $Ba_2CuGe_2O_7$ are compared with the corresponding infrared quantities, Ω_j^{IR}, Γ_j^{IR}, and S_j^{IR}, reported in Ref. [10] and with the frequencies Ω_j^{th} calculated by the shell model. All frequencies and widths are in cm^{-1}.

Phonon j	Symmetry	Ω_j^{th}	Ω_j^R [80 K]	Ω_j^R [300 K]	Γ_j^R [80 K]	S_j^R [80 K]	Ω_j^{IR} [7 K]	Γ_j^{IR} [7 K]	S_j^{IR} [7 K]
1	B_1	31							
2	E	59	55	53	7	<0.01			
3	E	75	99	99	1.5	0.02	84	2	0.13
4	E	108	105	104	1.5	<0.01	103	2	0.04
5	A_1	114	95	93	1.5	0.02			
6	B_1	121	112	112	1.5	<0.01			
7	A_1	123	121	118	1.5	<0.01			
8	E	129	131	130	2.5	0.12			
9	B_2	137					109	7	0.08
10	E	142	145		4	<0.01	152	7.5	0.07
11	B_1	149	143	141	4	0.04			
12	B_2	157					130	5	0.03
13	A_1	168							
14	E	179	193	191	2	<0.01	187	4	0.14
15	B_2	198					147	3	0.57
16	A_1	208	207	205	2.5	<0.01			
17	E	224					217	4	0.12
18	A_1	238	239	239	3.5	0.05			
19	E	258	259	257	3.5	0.09	257	21	0.15
20	E	261	281		3	<0.01	274	6	0.19
21	B_1	265	230	225	3	<0.01			
22	B_2	267					278	4	<0.01
23	B_2	318					321	10	<0.01
24	E	319	311	309	2	0.03	310	11	0.42
25	E	334	333	331	9	0.06	315	4	0.52
26	B_1	339	359		7.5	0.01			
27	B_1	373	372	370	4	0.01			
28	E	374	372	370	4	0.02	367	8	0.12
29	A_1	408	403	402	7	0.02			
30	B_2	412					390	15	0.27
31	E	443	436	437	10	0.03			
32	A_1	477	456	455	14	<0.01			
33	B_2	488					448	11	0.17
34	E	489	497	495	7	0.21			
35	A_1	517	515	517	14	<0.01			
36	B_2	559					488	9	0.35
37	E	766	740	736	4.5	0.10	710	7	1.00
38	B_1	773	780	780	3.5	1.00			
39	E	776	781	779	4.5	0.34	714	10	0.30
40	B_2	781					775	7	0.82
41	A_1	782							
42	E	786	809	804	4.5	0.28	772	8	0.02
43	B_2	794					791	17	0.40
44	A_1	797							
45	E	836					844	7	0.10

A_1 modes are allowed in both polarizations. Moreover, as the Raman microscope has a rather large numerical aperture, $\vec{E}$ has a small component along the crystal b axis, which can partially mix the ab-plane modes with those of the c axis. Nevertheless, one expects that the E modes of the ab plane are either absent or much weaker when $\vec{E}$ is along c. The former case is that of modes 2 and 37, and the latter one is that of lines 4 and 42, as one can see by comparing Figs. 2 and 3, where the intensities are on the same (arbitrary) scale. One thus obtains a first check of the assignment that is proposed in Table I. Given the high spectral resolution used in both experiments, the missing modes (three A_1, one B_1, and two E) are probably too weak to be observed.

After combining the 29 Raman lines observed here with the previous infrared observations, we could measure, and compare with the theoretical calculations, the frequencies and

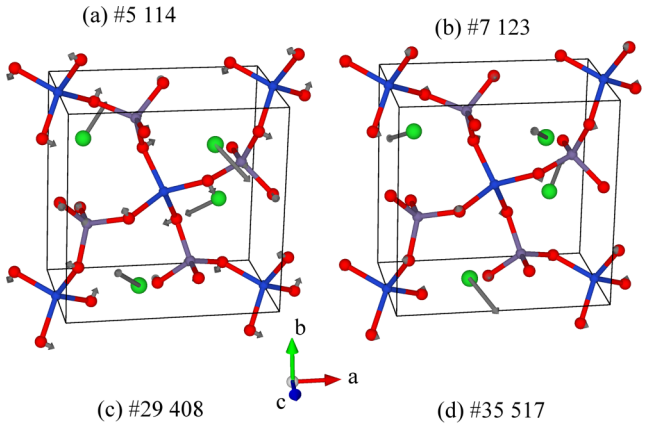

FIG. 4. (Color online) Atomic displacements for the $A1$ modes of $Ba_2CuGe_2O_7$. Each mode is identified by its number in Table I and by its calculated frequency, in cm^{-1}. Blue circles: Cu, Ge; red circles: O; green circles: Ba.

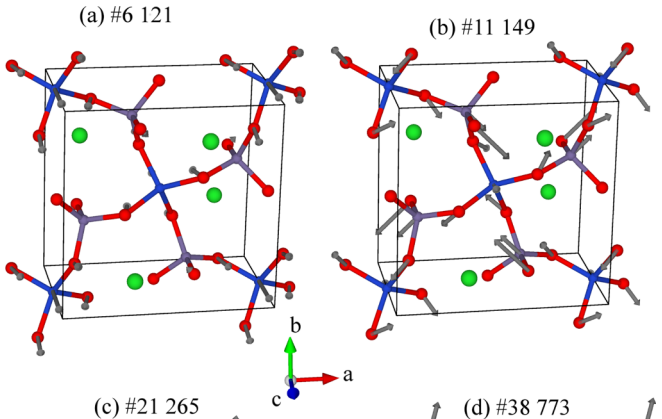

FIG. 5. (Color online) Atomic displacements for the $B1$ modes of $Ba_2CuGe_2O_7$. Each mode is identified by its number in Table I and by its calculated frequency, in cm^{-1}. Blue circles: Cu, Ge; red circles: O; green circles: Ba.

widths of 40 modes out of the 45 optical phonons predicted for $Ba_2CuGe_2O_7$. Concerning the evolution of the spectra with temperature, both Figs. 2 and 3 show at low T the usual narrowing of the lines but no meaningful increase in their intensity. This is at variance with the infrared absorption bands of BCGO, some of which become substantially stronger [10] for $T \to 0$, indicating a charge redistribution inside the BCGO cell. Such different behavior can be understood by considering that the matrix element of the infrared transition, unlike the Raman one, is driven directly by the dipole Hamiltonian associated with the lattice vibration.

The phonon frequencies Ω_j, widths Γ_j^R, and relative intensities S_j^R of the Raman lines, as extracted from the spectra of Figs. 2 and 3 through Lorentzian fits that are not shown in the figures as they practically coincide with the data, are listed in Table I. Each S_j^R value is proportional to the area of the jth Lorentzian, normalized to that of the strongest Raman line. For comparison, the corresponding infrared data at 7 K, where available (with S_j^{IR} normalized to that of the strongest IR line), and the theoretical frequencies obtained by the shell model (SM) are also listed. The latter calculations, which were described in detail in Ref. [10], are suitable for determining the lattice dynamics in compounds like the oxides in which the effects of the anion polarizability cannot be neglected [15,16]. Those calculations utilized the lattice constants and the atomic positions reported in Ref. [8]. The calculated frequencies of the A_2 silent modes, not reported in Table I, are 48, 125, 203, 341, 416, and 817 cm^{-1}. As one can see in Table I, the agreement between the theoretical calculations and the observed Raman frequencies is very good, with discrepancies which are only seldom larger than 10%. In order to evaluate the agreement with the infrared observations for the E and B_2 modes, one should consider that in the present backscattering configuration the Raman modes are longitudinal, while those observed in the infrared experiment at normal incidence are transverse. Moreover, the uncertainty for the infrared frequencies may be larger than for the Raman ones when several lines are close to each other. Indeed, in this case, the Kramers-Kronig procedure becomes less effective in separating the real and imaginary parts of the dielectric function, which are mixed with each other in the reflectivity spectra.

Concerning the Raman intensities, it is worth noting that some of the strongest Raman modes are also intense IR modes because the structure is highly noncentrosymmetric. Moreover, most of those lines are found at the vibrational frequencies expected for the CuO or the GeO bonds [around or above 500 cm^{-1}; see, e.g., mode 38 in Table I and Fig. 5(d)]. Indeed, the cross section for inelastic light scattering with creation of a phonon α is proportional to the Raman tensor, which is given by [17]

$$\left| \frac{\partial \epsilon_{\mu\nu}(\omega)}{\partial Q_\alpha} \right|^2 .$$

Here, $\epsilon_{\mu\nu}(\omega)$ is the dielectric tensor, Q_α parametrizes the phonon displacement, and the derivative should be evaluated at the energy of the incoming laser ($E_l = 1.96$ eV). This should not be too far from the charge-transfer (CT) band of the ligand O with the Cu ions (which in cuprates span from 1.5 to 2.5 eV [18]) and with the Ge ions. Even if E_l were not

resonant with the CT transitions but just close to them, the CT process would dominate the Raman matrix elements, as both the real and the imaginary parts of the dielectric function do contribute. Thus we expect strong Raman lines for the phonons which modulate the CuO or the GeO bonds, as shown in Figs. 2 and 3 and in Table I.

The atomic displacements corresponding to the most representative $A1$ and $B1$ modes are shown in Figs. 4 and 5, respectively. They are labeled by their number in Table I and by the theoretical frequency in cm^{-1}. Those corresponding to all the E and B_2 infrared-active phonons were already reported in Ref. [10]. As already noticed for the latter ones, in several vibrations the CuO tetrahedra and the GeO tetrahedra have a similar pattern due to the similarity of the Ge and the Cu masses. This accidental effect makes the tetrahedral "molecules" vibrate at similar frequencies and causes their modes in the crystal to mix appreciably.

III. CONCLUSION

In conclusion, we have presented the Raman spectrum of $Ba_2CuGe_2O_7$, an oxide which has recently attracted wide interest for the helical magnetism it displays at low temperature and for its peculiar multiferroic properties. We have observed 29 Raman lines which, once combined with our previous infrared observations, provide the frequencies, widths, and relative intensities at different temperatures of 40 phonon modes out of the 45 predicted by group theory for this crystal. These results, together with the shell-model calculations here extended to the Raman and silent vibrations, provide an exhaustive description of the lattice dynamics in $Ba_2CuGe_2O_7$. We hope that it may help us to better understand this oxide, which, in addition to its intriguing magnetic properties, displays interesting charge-lattice effects at low temperature in the infrared spectra.

ACKNOWLEDGMENTS

This experiment has been supported by the Università di Roma La Sapienza through the Progetti di Università 2013 and 2014. S.K. acknowledges support from the Consejo Nacional de Investigaciones Científicas y Técnicas (CONICET), Argentina.

[1] A. Zheludev, G. Shirane, Y. Sasago, N. Koide, and K. Uchinokura, Phys. Rev. B **54**, 15163 (1996).
[2] A. Zheludev, S. Maslov, G. Shirane, Y. Sasago, N. Koide, and K. Uchinokura, Phys. Rev. B **57**, 2968 (1998); A. Zheludev, S. Maslov, G. Shirane, I. Tsukada, T. Masuda, K. Uchinokura, I. Zaliznyak, R. Erwin, and L. P. Regnault, *ibid.* **59**, 11432 (1999).
[3] J. Chovan, M. Marder, and N. Papanicolaou, Phys. Rev. B **88**, 064421 (2013).
[4] I. E. Dzyaloshinskii, J. Phys. Chem. Solids **4**, 241 (1958).
[5] T. Moriya, Phys. Rev. **120**, 91 (1960).
[6] A. Zheludev, T. Sato, T. Masuda, K. Uchinokura, G. Shirane, and B. Roessli, Phys. Rev. B **68**, 024428 (2003).
[7] H. Murakawa, Y. Onose, and Y. Tokura, Phys. Rev. Lett. **103**, 147201 (2009).
[8] M. Tovar, R. E. Dinnebier, and W. Eysel, Mater. Sci. Forum **278-281**, 750 (1998).
[9] K. Momma and F. Izumi, J. Appl. Crystallogr. **44**, 1272 (2011).
[10] A. Nucara, W. S. Mohamed, L. Baldassarre, S. Koval, J. Lorenzana, R. Fittipaldi, G. Balakrishnan, A. Vecchione, and P. Calvani, Phys. Rev. B **90**, 014304 (2014).
[11] P. Calvani, M. Capizzi, S. Lupi, and G. Balestrino, Europhys. Lett. **31**, 473 (1995).
[12] R. Fittipaldi, L. Rocco, M. Ciomaga Hatnean, V. Granata, M. R. Lees, G. Balakrishnan, and A. Vecchione, J. Cryst. Growth **404**, 223 (2014).
[13] A. L. Glebov, O. Mokhun, A. Rapaport, S. Vergnole, V. Smirnov, and L. B. Glebov, Proc. SPIE **8428**, 84280C.
[14] Bilbao Crystallographic Server, http://cryst.ehu.es/rep/sam.html; E. Kroumova, M. I. Aroyo, J. M. Perez-Mato, A. Kirov, C. Capillas, S. Ivantchev, and H. Wondratschek, Phase Transitions **76**, 155 (2003).
[15] S. Koval, R. Migoni, and H. Bonadeo, J. Phys.: Condens. Matter **4**, 4759 (1992).
[16] J. Lasave, J. Kohanoff, R. L. Migoni, and S. Koval, Phys. B (Amsterdam, Neth.) **404**, 2736 (2009).
[17] *Light Scattering in Solids II*, edited by M. Cardona and G. Güntherodt, Topics in Applied Physics Vol. 50 (Springer, Berlin, 1982).
[18] D. N. Basov and T. Timusk, Rev. Mod. Phys. **77**, 721 (2005).